Analyses of Blue Origin Blue Moon Lunar Landing Descent Engine Plume Effects

William A. Hoey[1], Maxwell G. Martin[2], John M. Alred[3] and Carlos E. Soares[4]
Jet Propulsion Laboratory, California Institute of Technology, Pasadena CA 91109, USA

Mohammed T. Ababneh[5]
Blue Origin, LLC, Kent WA 98032, USA.

Powered landings onto airless bodies like the Moon generate rarefied gas dynamic environments composed of engine plume flows and surface materials including mobilized dusts. These induced atmospheres can cause harmful degradations of spacecraft performance. In particular, lunar dust can cause severe operational problems for human and cargo landing systems, astronauts, and deployed scientific observatories as was observed during the Apollo program. The need to understand and quantify the effects of plume-surface interactions during powered landings onto airless bodies has motivated the development of physics-based modeling approaches at NASA's Jet Propulsion Laboratory. JPL incorporates inputs from Blue Origin and literature surveys of lunar regolith and applies computational fluid dynamics, direct simulation Monte Carlo, and Lagrangian particle-tracing simulation methodologies to model the plume exhaust flowfields generated by the Blue Moon descent engines during the final meters of landing, as well as the effects of that plume flow in eroding, entraining, and transporting lunar regolith to the descent element. The effects of dust deposition onto thermal control system radiators are of primary interest in this work, but other detrimental effects can include deposition onto landing sensors and optical systems during and after landing; damage induced by dust impact or subsequent abrasion within exposed lander cavities; and the performance degradation of solar arrays and scientific payload instruments. Plume interactions will also result in lunar dust clouds which may obscure visibility during landing, and may cause mechanical erosion of surfaces downstream of the plume-surface interaction.

Nomenclature

α	=	absorptivity
CFD	=	computational fluid dynamics
DDL	=	deorbit, descent and landing
DSMC	=	direct simulation Monte Carlo
Kn	=	Knudsen number
PAC	=	percent area coverage
PSI	=	plume-surface interaction

I. Introduction

AS Blue Origin's Blue Moon lander approaches and touches down on the Moon, how will its descent engine plumes interact with the lunar surface, and what effects might lunar dust have on the lander? The self-induced contamination of lunar landing vehicles, combined with the natural lunar environment, can adversely impact the performance of critical engineering systems (i.e. thermal control; power generation; sensors; mechanical systems and actuators) and of payloads including mission cargo and science instrumentation. Characterization and mitigation of

[1] Technologist, Contamination Control Engineering, <william.a.hoey@jpl.nasa.gov>, MS 125-109.
[2] Systems Engineer, Contamination Control Engineering, <maxwell.g.martin@jpl.nasa.gov>.
[3] Technologist, Contamination Control Engineering, <john.m.alred@jpl.nasa.gov>.
[4] Principal Engineer, Group Supervisor; Contamination Control Engineering, <carlos.e.soares@jpl.nasa.gov>.
[5] Thermal Control Systems Lead & Thermal/Fluid Systems Architect, <mababneh@blueorigin.com>.

landing vehicle self-induced contamination is therefore essential to mission success and to ensuring the safety and performance of lunar mission cargo and science assets.

Lunar landing events can induce many adverse effects.[1-4] Powered landings onto 'airless' bodies – bodies without continuum, collisional atmospheres at their surface, e.g. Earth's moon – generate rarefied-gas environments.[2-9] These environments are composed primarily of propulsion byproducts in expanding engine plumes and surface materials, e.g. mobilized regolith and dust, persisting above landing sites for at least the duration of powered landing. Such spacecraft-induced 'atmospheres' are many orders of magnitude more dense than unperturbed ambient environs,[7,8] resulting in contamination impacts to mission science and engineering objectives. Key vectors for such contamination include the gas- and liquid-phase byproducts of chemical propulsion that constitute descent engine plumes,[10] and materials mobilized and transported within the ephemeral, plume-induced rarefied environs created by landing.[1-4,9] Lunar regolith and dust can cause severe operational problems for human and cargo landing systems, astronauts and deployed scientific observatories.[1,3,4,9-12] Such material instigated by landings and human activities on the lunar surface was more problematic than anticipated during the Apollo program: Apollo missions were adversely affected by visual obscuration during and after landing; the abrasion and erosion of surfaces by plume-induced ejecta; false instrument readings; thermal control problems; dust coating and contamination effects including seal failures and the clogging of mechanisms; losses of traction against the lunar surface; and human effects including lung irritation.[11] Lunar missions may expect to experience particularly adverse effects during landings as landing sites are eroded by descent engines. Spacecraft instruments and other sensitive surfaces, i.e. thermal control system radiators and solar panels, may be impacted by the direct impingement or fallout of particles removed from the landing surface by descent engine plumes and by the accumulation of gas- and liquid-phase engine plume byproducts. For these reasons, the Jet Propulsion Laboratory (JPL) has pursued a multi-disciplinary effort to characterize and simulate the physics and contamination effects of powered descent onto airless bodies, and to inform design choices and operational mitigation strategies.

This manuscript addresses an engineering model framework developed and applied by JPL from 2019−2020 to simulate Blue Origin Blue Moon descent engine plumes and their effects on the vehicle and its landing site surface, including treatment of multi-regime continuum, rarefied and free-molecular gas flows and induced regolith viscous erosion. Section II of the manuscript describes the simulation methodologies applied in this model framework, while Section III describes the essential inputs to and boundary conditions of such a framework and Section IV contains notes toward the selection of simulation case matrices for generic lunar landings. Section V details the conclusions of the continuum CFD, coupled CFD-DSMC, and erosion and particle transport models during a representative Blue Moon landing sequence. Section VI ends the paper with conclusions related to the specific instance of a Blue Moon landing and additional lessons-learned for the simulation of other generic lunar landing processes and induced effects.

II. Methodology

Descent engines and, to a lesser extent, reaction control system thrusters will be primary sources of vehicle and landing site contamination during lunar landing events. Plume flows into vacuum are inherently multi-regime, starting as continuum flow within nozzles and immediately downstream of the nozzle exit.* As plumes expand into vacuum, intermolecular collisions become infrequent as flows transition through the rarefied gas dynamic and into the free-molecular regime. As a spacecraft approaches a landing site surface on an airless body, its engine plumes may form a rarefied or continuum region above the plume impingement point as they interact with the surface. Complex flow structures incorporating surface material can emerge around this plume impingement point in the family of *plume-surface interaction* (PSI) – an active area of research. Lunar landing plume flows have been predicted and observed to create a region of low density, high velocity gas flow along the surface at low angle that entrains and transports eroded surface particulate at km/s speeds.[1-5,9,12,17-19] Such particles can cause mechanical damage to exposed vehicle elements e.g. legs and footpads, but also to distant structures as observed when the Apollo 12 landing induced a 'sand-blasting' of exposed surfaces on the Surveyor 3 probe.[1,12] For denser plume flows at low altitudes and especially for multi-engine landings, recirculation structures may form that transport eroded surface materials toward the vehicle.

A. Simulation Techniques for Continuum and Rarefied Flows

Computational fluid dynamics (CFD) techniques can be used to simulate engine plume flows in their entirety in wholly-continuum environments by solving e.g. the Navier-Stokes partial differential equations. However, continuum

* Although complicating rarefaction effects may occur within nozzles expanding into vacuum, particularly at the nozzle lip, such effects are neglected for the engineering purposes described in this manuscript.

fluid dynamic models fail for gases of sufficiently low density as "gradients of the macroscopic variables become so steep that their scale length is of the same order as […] their mean free path."[13] Continuum assumptions begin to break down as the Knudsen ratio of mean free path to flow characteristic length scale, *Kn*, exceeds approximately 0.1. The direct simulation Monte Carlo (DSMC) method is a useful and standard approach for modeling a wide range of continuum-to-rarefied-to-vacuum flows, and is applied here to represent plume gas expansion into the near-vacuum lunar environs beyond the nozzle near-field regime. DSMC is a Lagrangian and probabilistic technique by which 'real' molecules are represented with some small proportion of simulated molecules.[13] These simulated molecules can move, collide with surfaces, and experience various physics as would their 'real' counterparts. However, their intermolecular collisions are not deterministic, but instead occur stochastically within an imposed mesh. DSMC is most useful where gas flows transition from continuum into rarefied and free-molecular regimes, but the technique remains valid (albeit computationally expensive) in continuum regimes if mean-free-paths and collision time-scales are resolved.

The need to understand and quantify the effects of plume-surface interactions during powered landings onto airless bodies has motivated the development of hybrid CFD-DSMC coupled schemes by JPL spacecraft engineering teams. Standard engineering approaches apply mature commercial software, e.g. Siemens Simcenter STAR-CCM+, for continuum solutions that are one-way coupled at domain interfaces into a DSMC package. The NASA DSMC Analysis Code (DAC)[14] has been used extensively in analyses of multi-engine plume-impingement problems for International Space Station (ISS) docking in near-vacuum regimes,[15] and is in general use by NASA flight project engineers for analyses of spacecraft plume-plume and plume-structure interactions. For lunar landing applications, Morris et al. (2015a) demonstrated hybrid one-way-coupled CFD-DSMC simulations of plume impingement onto the lunar surface for the Apollo lunar module descent engine (LMDE) system; these cases have been used by Lam et al. (2019) to cross-validate a JPL hybrid approach that couples STAR-CCM+ and DAC.[6] The LMDE, a throttled hypergolic engine that used an N_2O_4 oxidizer and Aerozine 50 fuel mixture, formed the descent propulsion system for Apollo-program lunar landings—it is a useful comparison case as its nozzle contour, ideal exhaust mixture, throttling and performance during Apollo landings are known; this is discussed further by Morris et al. (2015a) and authors including Lam et al. (2019) and Rahimi et al. (2020) that compare LMDE simulation results against Morris. The CFD-DSMC approach of Lam et al. (2019) was extended by the authors to multi-engine-plume cases with vehicle envelopes for the NASA Europa Lander mission concept,[7] and this forms the basis of the gas dynamic simulation approach applied in this manuscript.

B. Lunar Viscous Erosion Processes and Particle Transport

When landings occur onto granular material, as for the Moon, plume-surface interaction (PSI) phenomena may induce the erosive removal and transport of particle matter. Several erosive and crater-formation mechanisms have been studied for PSI applications in continuum environments (i.e. Earth and Mars) and also for the Moon.[16,17,18] The primary erosive mechanism for lunar landings was theorized[17] and has been observed to be *viscous erosion* for landers as large as Apollo, which had throttled its main engine to 13.3 kN during its final landing sequence.[2,3,5,9,18] Viscous erosion is the process by which plume-induced shear stress exceeds inter-particle cohesion on an impingement surface, resulting in a 'sweeping' of particles from the surface; particle-particle collisions then lead to a lofting and entrainment of particles within the plume flowfield.[5] Several models for lunar landing viscous erosion have been proposed, including shear stress formulations following the pre-Apollo Roberts form[17] which have since been revised to better align with observations by Apollo[19] and subsequent[9] lander programs, and dynamic pressure formulations calibrated to Apollo data.[2,5] With such models, plume flowfield simulation data from continuum-rarefied solvers (e.g. CFD-DSMC) can be applied directly to calculate surface erosion rates and the morphology of PSI-induced craters formed throughout a landing sequence.[3,5,9] Flowfield solutions and viscous erosion models can also be linked to inform the generation and transport of simulated particles within a Lagrangian framework, enabling engineering teams to address questions related to particulate impingement and deposition. The JPL in-house particle transport and deposition tool applied in this manuscript, SPLAT, extends a tool introduced by Brieda (2018) and applied by Anderson et al. (2020) in steady and transient transport analyses with spacecraft contamination control and systems engineering applications.

C. An Engineering Framework for Modeling Lunar Landing Effects

Spacecraft engine plumes and plume-surface interactions relevant to lunar landings are complex and inherently multi-regime; models that would characterize such phenomena for engineering applications must hold validity across continuum, rarefied, and free-molecular gas dynamic regimes and must incorporate treatments for regolith erosion and particle transport. Likewise, models for engineering use must incorporate detailed geometric representations of landing sites and vehicles, and must be computationally tractable at a scale that permits analysis of robust case matrices and the evaluation of design trades. While models and simulation techniques exist that offer one or several such capabilities, no comprehensive and integrated model framework has been introduced for application to the design of

lunar landing vehicles. Therefore, JPL developed an engineering model framework to one-way-couple gas dynamic, surface erosive, particle transport, and optical property degradation models for application to a Blue Moon landing. Figure 1 identifies the discrete inputs required for each step in the analysis workflow, and defines how each subsequent model in the workflow ingests outputs from prior steps. Starting from engine performance details provided by Blue Origin at either nozzle throats or exit planes, the initial analysis step generates near-field CFD simulations that define inflow boundary conditions for three-dimensional DSMC cases. These cases, performed at altitudes and throttlings representative of a planned Blue Moon descent, describe plume expansion into vacuum and include effects of plume-plume and plume-surface interactions with the Blue Moon vehicle and landing site surface. Flowfield results are linked with empirical models to estimate the effects of regolith viscous erosion in crater formation and the removal of particles from the lunar surface. Representative particles are then transported throughout the simulation domain, and interact with landing site and vehicle surfaces, in an application of the JPL in-house Lagrangian tool SPLAT. Particle depositions predicted by this tool are converted to thermal and optical performance degradations as final outputs of the model framework. Section III reviews necessary model inputs and the analysis workflow in detail.

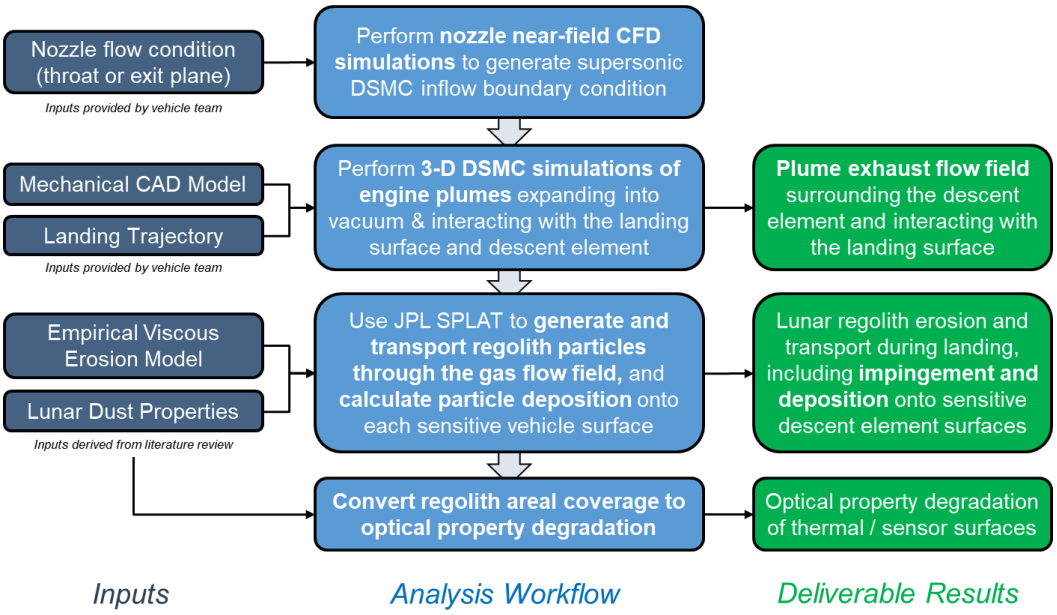

Figure 1. JPL lunar landing plume-surface interaction engineering analysis framework.

III. Input Information

A. Blue Moon Engine Conditions

JPL performs STAR-CCM+ CFD simulations of nozzle flow to generate gas field solutions for the engine exhaust plume expansion into near-vacuum; plume self-interaction, as the modeled Blue Moon descent element features two engines; and plume interactions with the descent element and lunar surface during landing. CFD simulations reviewed in this manuscript begin at the exit plane of a converging-diverging nozzle using a set of thermodynamic properties provided by Blue Origin for a relevant range of engine throttling conditions.

B. Blue Moon Descent Element Geometric Model

A simplified version of the as-delivered Blue Moon descent element geometric model was created to reduce mesh complexity, which improves the efficiency of DSMC and particle-transport analyses. A combination of point-cloud and model measurements were used to recreate most descent element surfaces, from landing feet to the top of radiator surfaces and solar reference units (SRUs). The model reduction process preserves contamination-sensitive surfaces susceptible to degradation and other surfaces that effect plume flowfields, but simplifies or eliminates other unnecessary surface, interface, and curvature complexity. After completion, the reduced JPL model was overlaid with

the as-delivered Blue Origin CAD model to check for any geometric inconsistencies. As seen in Fig. 2, the reduced model shows excellent correlation with the as-delivered CAD model. In this example case, the reduced model was generated and DSMC and regolith-transport simulations performed fully in 3-D to preserve the asymmetry of radiator placement in the descent element design.

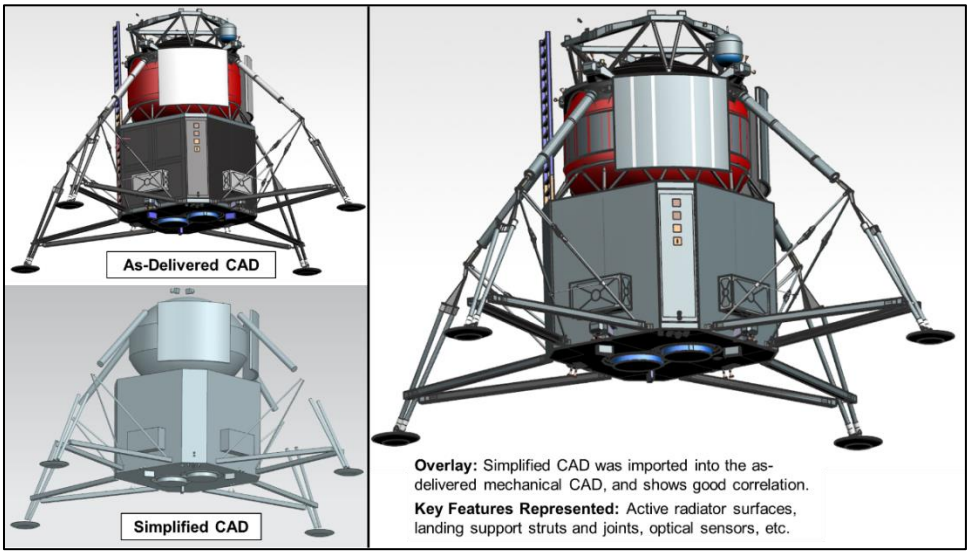

Figure 2. Detailed and reduced CAD models for a Blue Moon descent element in a dual-engine configuration.

C. Blue Moon Landing Trajectory

For the example set of analyses, Blue Origin provided JPL an engine throttling-vs-altitude profile and a deorbit, descent and landing (DDL) trajectory, which are used to set throttling cases for each snapshot altitude and to integrate erosion results vs. time. This example assumes a steady descent of ~1 m/s at ~30 % throttle below 11 m altitude.

D. Lunar Regolith Empirical Viscous Erosion Model

Metzger et al. (2008, 2010); Morris (2012) and Morris et al. (2015a); and Rahimi et al. (2020) provide thorough overviews of various regolith erosion mechanisms that occur in lunar landing regimes contingent on environmental boundary conditions. Based on known lunar regolith properties, e.g. high bearing strength and packing density, the absence of an atmosphere on the moon and Apollo-era descent and landing observations, the viscous mechanism is understood to be the primary cause of plume-induced regolith erosion during lunar landings up to Apollo scale, with other mechanisms generally treated as negligible by comparison. Viscous erosion – by which shear stress exerted on a landing surface causes loose grains to slip or roll along that surface, collide with other grains, and ultimately entrain within a plume flow – was modeled prior to the Apollo lunar landings with analytical methods like the treatment of Roberts (1963). Those methods were refined by Metzger et al. (2008), who performed testing of plumes impinging on dusty surfaces across several pressure and gravity regimes to motivate an empirical model applicable to lunar regolith erosion.[18,19] A related model was proposed and applied in DSMC simulations of Apollo lunar landings by Morris (2012) and Morris et al. (2015a) in a dynamic pressure form scaled to match analysis of Apollo landing imagery; a similar model was applied in the Blue Moon study.

E. Lunar Regolith Properties

For the assessments addressed in this manuscript, size distributions, densities and thermo-optical properties of lunar surface material were drawn from literature review. At that time (2019−2020) a landing site had not yet been finalized for Blue Moon, so no attempt was made to select or tailor regolith properties to a specific lunar region; instead a range of regolith and simulant properties was considered in an effort to bound potential landing-induced degradation effects. Particle size distributions in the reviewed literature were generally presented in weight or volume fractions but specific particle counts were available for some samples that enabled calculation of relative count fractions for each particle size.[22,23] Particle size distribution count fractions as reported in Table 1 were used in the particle transport and thermo-optical degradation effect portions of the engineering model framework. Measured

values of lunar regolith and regolith simulant thermo-optical properties presented a range of absorptivity (0.39−0.75) and emissivity (0.78−0.92) values that defined best- and worst-case cases for e.g. radiator performance degradation.[24]

NASA provides a relevant design specification for lunar regolith properties in engineering applications; the Cross-Program Design Specification for Natural Environments derives thermo-optical property values from measurements collected by the Lunar Reconnaissance Orbiter (LRO).[25] Revision I of the specification, dated Oct. 2021, reports emissivity values of 0.95−0.98 in lunar Mare and Highland equatorial and in South Polar (84 to 90°S) regions alike. Regolith absorptivity (α) is not directly reported but can be calculated by subtracting albedo from 1—values range from 0.84 in Highland and South Polar regions to 0.93 in Mare regions. Section V of this manuscript reports changes in absorptivity, emissivity, and their ratio for an example radiator surface under various partial coverage conditions using first the range of regolith and simulant properties derived from literature review as applied in Blue Moon assessments (Table 2), and then updated for South Polar regolith conditions per the Rev. I specification (Table 3).

Table 1. Lunar regolith size distribution data normalized to number of counts in each particle size bin.

Source	<20 µm	20-45 µm	45-75 µm	75-90 µm	90-150 µm	150-250 µm	250-500 µm
Lunar Soil 15601, 96a	-	18 %	19 %	18 %	18 %	18 %	9 %
*Soil 71061,1**	18 %	10 %	18 %	18 %	18 %	11 %	8 %
Soil 72441,7f	20 %	11 %	16 %	17 %	20 %	10 %	6 %
Soil 64501	-	18 %	17 %	17 %	17 %	17 %	13 %

IV. Simulation Case Matrices

An engineering analysis program for plume-surface interactions and induced contamination effects must carefully assess the planned deorbit, descent and landing (DDL) profile of a lunar lander and respond to nominal and edge cases. During the study described in this manuscript, several descent element configurations were considered – e.g. single-vs.-multiple engine – as were worst-case landing site surfaces including maximum permissible slopes and extant natural crater features. Results are shown for a study of landings onto planar surfaces as steady-state CFD-DSMC snapshots generated with nozzle exit planes at 10, 5, 3, and 1.5 meters above the landing site. These displacements (referred to as 'altitudes' throughout Section V) are matched to engine throttling levels and vehicle descent velocities drawn from a representative DDL example. The selection of incremental steady-state snapshots is consistent with other approaches in the literature,[3,5-9] and is supported by the steep difference in time-scales between flowfield gas dynamic and particle motion on the order of ~1 km/s and vehicle motion ~1 m/s. Macroscopic landing site deformation due to Blue Moon plume-induced viscous erosion was anticipated to result in formation of broad, shallow 'crater' features no greater than several cm in depth, consistent with Apollo and subsequent lander observations and insignificant in comparison to anticipated natural surface feature scales that would otherwise alter a plume flowfield.

V. Simulation Results

A. CFD Analysis: Continuum Near-Field and Plume-Plume Interactions

JPL performed STAR-CCM+ CFD simulations of nozzle interior and near-field flow to simulate continuum regime flow, and began these simulations at the exit plane of the converging-diverging nozzle using a set of thermodynamic properties for relevant engine throttling conditions. The CFD results shown here were generated in a steady-state, axisymmetric domain assuming laminar supersonic flow. The backflow domain is held at the lowest possible pressure (< 100 Pa) to facilitate as realistic an expansion as possible into the near-vacuum lunar domain. Mesh convergence studies found a 1 mm initial cell length with wall refinement to be suitable; residuals were converged to below 10^{-5} in all relevant relative metrics. The gas flow represented is fully non-reactive H_2O with real-gas thermodynamic models including variations of specific heat and viscosity with temperature.

B. Coupled CFD-DSMC Analysis: High-Altitude Free Expansion

Following high-resolution and adaptively-meshed simulations of dual-engine plume near-field interactions in free expansion, JPL considered free-expansion in an extended 10 m × 20 m × 20 m domain inclusive of the descent element model. These results may be used to estimate the onset height of regolith erosion and transport phenomena – peak dynamic pressure and therefore peak viscous erosive rates are calculated and extrapolated along the descent axis.

Apollo observations found the onset height of visible erosion to be ~30−40 m. The lunar environment is a near-perfect vacuum in which engine plume flows can expand freely beneath the descent element until they interact with each other, with vehicle structures or the lunar surface. When adjacent engine plume flows interact in vacuum they may create a collisional high-density, high-temperature region between them in which complex flow structures form. A plume-plume interaction is shown in Fig. 3 in a 3-D, steady-state result at 'high altitude' without a landing surface.

C. Coupled CFD-DSMC Analysis: Blue Moon Landing Flowfield Simulations

In the example case matrix described in this manuscript, flow from two engines at steady throttling impinges onto planar lunar surfaces in four increments starting at 10 m altitude, measured by nozzle exit plane elevation above the lunar surface, until engine shutdown at a minimum footpad altitude of ~1 m. Nozzle CFD results pass into the DSMC rarefied-gas dynamic domain across a one-way coupling interface, along which macroscopic flowfield properties are translated into simulated molecules with related, Maxwell-distributed properties. The coupling interface is drawn such that flow into the DSMC domain is always supersonic normal to the boundary and at as high a Knudsen number (*Kn*) as feasible within the continuum domain to reduce DSMC computational expense – even so, flowfields shown cost ~100,000 CPU-hrs. each using the JPL Gattaca supercomputing cluster. Figure 4 shows a representative result for a dual-engine Blue Moon configuration at 10 m altitude on symmetry cut-planes at $X = 0$ and $Y = 0$, colored by pressure.

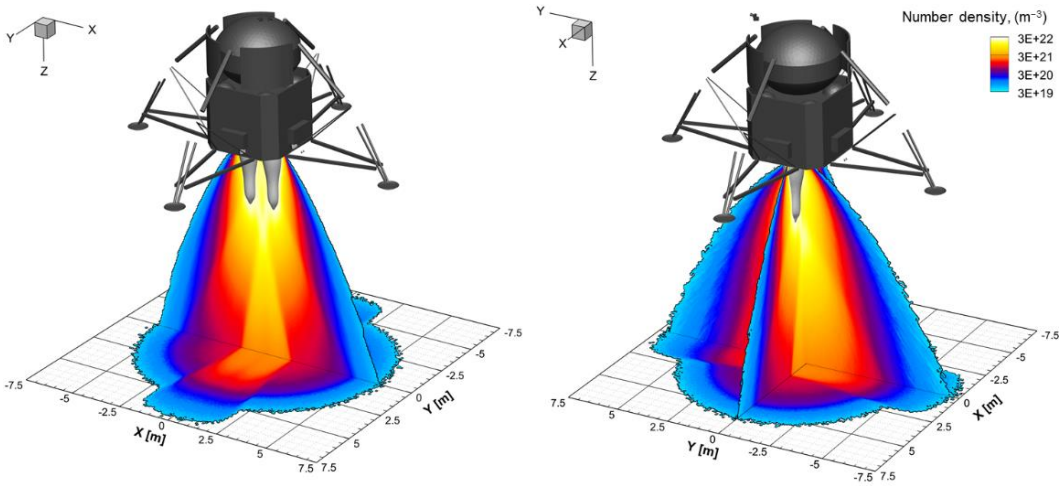

Figure 3. Blue Moon dual-engine plumes expanding freely into vacuum, colored by number density.

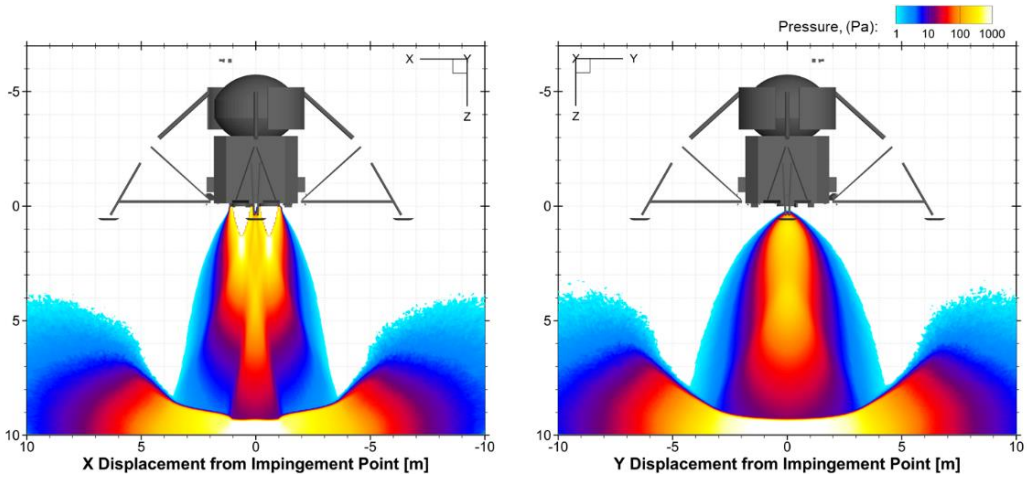

Figure 4. Blue Moon dual-engine plumes at 10 m altitude onto a flat planar landing site, colored by pressure.

An interesting axis-switching feature is observed in the free-expansion case of Fig. 3 as plume exhaust expands most broadly in the Y-Z plane, perpendicular to the X-Z plane that holds both nozzle centerlines. For a dual-engine Blue Moon configuration, plume-plume interactions tend to drive gas outward in the ±Y-directions where little plume gas and no ambient gas exists to restrict plume expansion. Both the free-expansion case of Fig. 3 and the 10 m altitude case of Fig. 4 apply vacuum domain boundaries; however, plume gas interaction with the ground plane has the effect of restricting expansion in the latter case. Axis-switching has been observed for non-axisymmetric plume flows even in continuum conditions but the effect is exacerbated in vacuum. It has been studied for other rarefied plume flows, for instance in multiple-engine lunar landing cases by Morris et al. (2015b) who likewise observed that such flows are "focused near the symmetry plane between adjacent nozzles," and also in cases of long rectangular or arbitrarily-shaped vents exhausting into vacuum in volcanic plume flows.[26,27] For landings of vehicles with multiple engines arranged in non-axisymmetric configurations, axis-switching will be observed in plume-surface interactions as well.

Compared to sloped surfaces, planar flat surfaces present a worst-case for induced pressures as both nozzle exit planes reach a minimum altitude of 1.5 meters. Planar flat surfaces were not found to be a worst-case configuration for vehicle regolith impingement, however, as they do not represent surface features that tend to deflect lofted particles upward. Both sloped and cratered surfaces were analyzed; an example for landing onto a worst-case planar sloped site is shown as Fig. 5. Similar results were used to predict plume-induced pressures onto vehicle surfaces. Estimated pressure loads onto descent element surfaces were assessed for compatibility against vehicle structural elements, e.g. aluminum, steel, titanium, carbon composites, and MLI. As expected, plume-induced pressures increase rapidly as Blue Moon approaches the surface and peak for the case at minimum 1.5 m altitude. An example of Blue Moon plume-induced pressure loads onto descent element surfaces at 1.5 m altitude in a flat planar landing is shown in Fig. 6.

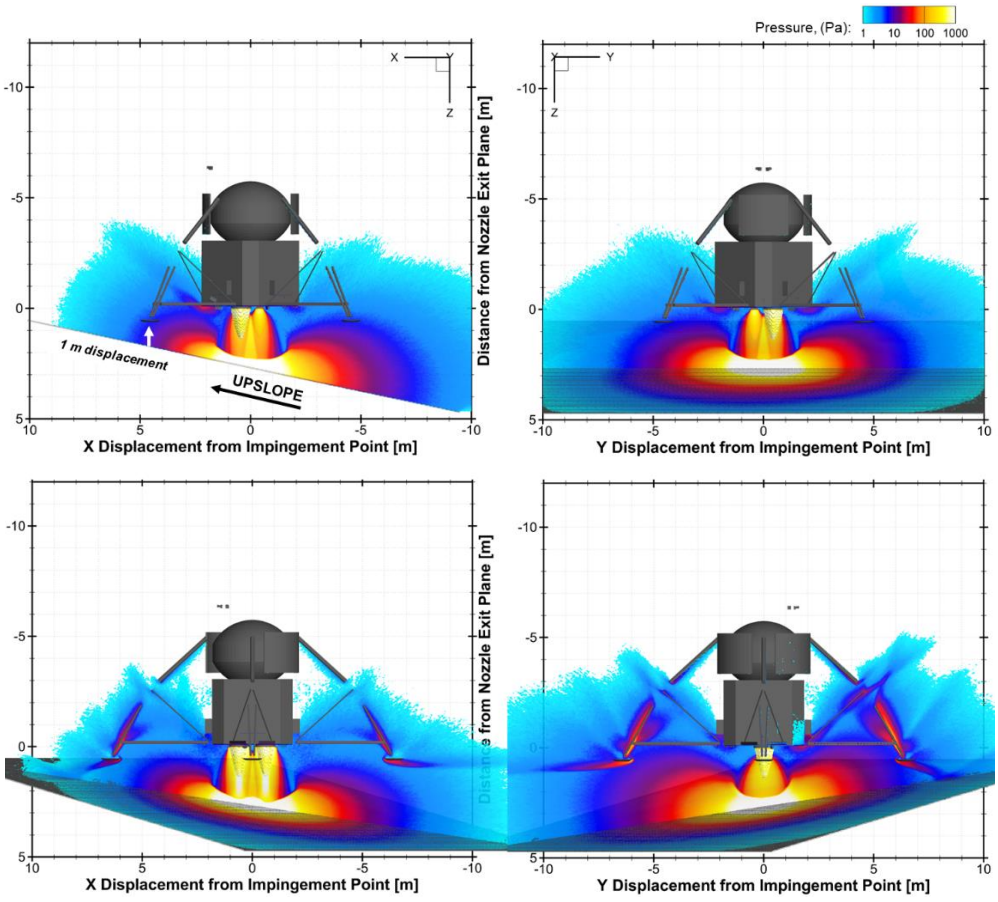

Figure 5. DSMC result for Blue Moon dual-engine plume interactions onto a sloped landing site relative to the descent axis with footpad minimum displacement 1 m. Slices are colored by pressure. Each panel shows a different slice through the same flowfield; panels at top align with the sloped surface; panels at bottom are offset 45° from the top panels and align with the nozzle centerline plane and the descent element footpads.

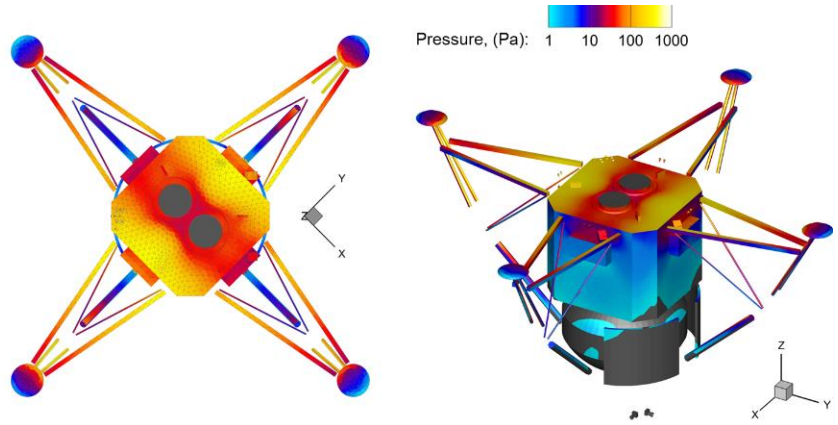

Figure 6. DSMC solutions for Blue Moon showing plume-induced impingement pressures at 1.5 m altitude.

D. Instantaneous and Integrated Surface Viscous Erosion

JPL applied the empirical model outlined previously to calculate regolith erosion via the viscous mechanism as a function of dynamic pressure at the boundary layer. The results of this assessment do not project a 'large crater' to form during the simulated Blue Moon landings; instead, exposed and loose lunar regolith would be removed from the landing site by engine plume flows during final descent, beginning at ~30−40 m altitude and increasing rapidly in erosion rate with descent element proximity to the surface. Peak point erosion rates may surpass 1 cm/s at engine shutdown. On the lunar surface, most erosion will occur within 10 m radially of the descent axis, with morphology consistent with Apollo landing observations and dominated by viscous erosion. A shallow, elliptical crater with peak depth of several cm may form beneath the descent engines with its major axis aligned with the dual engines – as observed in the Apollo landings, JPL observes peak simulated plume-induced crater depth to form about 1 m away from the descent axis, albeit with a more complex distribution than observed for Apollo given plume-plume interaction in this dual-engine configuration. In comparing Blue Moon erosion profiles to results in the literature and in validation simulations for the Apollo LMDE, e.g. Morris et al. (2015a), Lam et al. (2019), Rahimi et al. (2020) vs. Blue Moon at 5 m, there may be a secondary effect in the dual-engine configuration as plume-plume interaction promotes the spreading of flow along the engine layout minor axis. Additional regolith will be removed by processes not considered in this assessment, i.e. above 11 m (for which an estimate may be extrapolated from existing cases) and as the descent element operates its engines below the minimum simulation altitude of 1.5 m including time taken to throttle down.

E. Particle Transport and Impingement in a Dual-Engine Analysis

As a lunar landing vehicle descends, its engine plumes impinge on the lunar surface and promote the sweeping-up and transport of regolith and dust particles within the interacting plume-surface flowfield. A fraction of mobilized particles will impinge on vehicle surfaces; impinging particles can produce deposits on sensitive surfaces in the case of *attachment*, which can be enhanced by electrostatic charges produced by solar wind interaction with the regolith layer. Particles that accumulate on Blue Moon sensitive surfaces would alter thermo-optical properties as lunar regolith exhibits high solar absorptance and high IR emittance, and would also affect performance of optical systems by obscuration and scattering of light. Particles that are accelerated to flowfield velocities, on the order of ~1 km/s, can also cause *mechanical erosion*. Coupled CFD-DSMC flowfield solutions for a dual-engine configuration of the Blue Moon descent element were used as inputs to a Lagrangian model of particle mobilization, transport, and vehicle impingement. In this model, flowfield results at each altitude snapshot were used to estimate instantaneous and integrated values for regolith erosion, transport, and accumulation onto the Blue Moon descent element. Lagrangian simulations were performed with JPL in-house software for ~10^6 simulated 'macro-particles' per case, as simulating an actual number of eroded regolith particles would be intractable. Macro-particles were weighted to represent quantities of eroded regolith in a particular size class with reference to a regolith size distribution (e.g. as Table 1). Erosion of lunar regolith and subsequent transport were then integrated over the landing trajectory to obtain estimates of area coverage for different descent element components. An example of sampled Lagrangian particle trajectories is shown in Fig. 7 at 3 m altitude; note the dust-vehicle interactions, in this case modeled as elastic collisions. During example integrated landing sequences from 10 to 1.5 m altitude aft panel and active radiator surfaces were tracked as primary deposition-sensitive surfaces along with leveling mechanisms, landing sensors and optical systems.

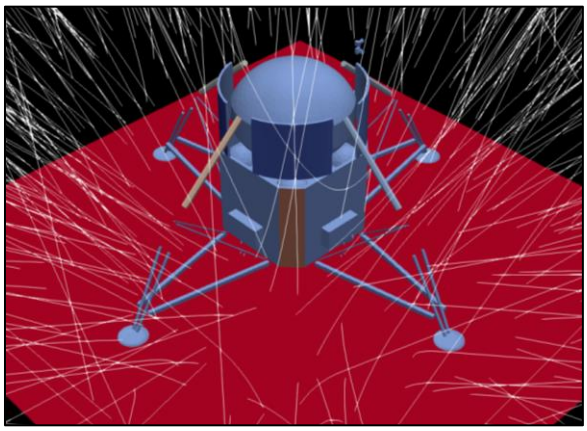

Figure 7. An example of lunar regolith transport for a Blue Moon landing case at 3 m altitude onto a flat and smooth planar landing site surface. The white traces show 1,000 example trajectories drawn from a total of 10^6 simulated macro-particle samples (i.e. 0.1 % of sampled trajectories are visible). In this example, each macro-particle itself represented ~10^6 actual regolith particles within a discrete size bin.

A range of particle initialization conditions was considered. First, detachment velocities were set to match surface-tangential velocities above the boundary layer at ~500 m/s, with particles released from a cosine angular distribution. This mode of detachment was intended to capture interactions with immovable surface roughness features at the scale of the boundary layer observed during the Apollo landings, e.g. streaking effects visible during the Apollo 15 landing. However, this mode was found to generate peak spray angles in excess of the maximum 8.1° observed during Apollo landings. In response, detachment velocities and release angles were controlled to achieve an 8.1° spray angle with velocity ~70 m/s. While the same amount of surface material was eroded in each set of cases, the decrease in particle detachment velocity and therefore in peak spray angle promoted less particle transport to the descent element in the latter set of cases. The work described in this manuscript studied plume interactions with smooth planar landing sites, either flat, as in Figs. 4 and 7, or sloped as in Fig. 5. Further assessments of landing site surfaces with realistic large-scale topologies or small-scale roughnesses were out of the scope of this effort, excepting one case that assessed a single pre-existing crater (a defined 'worst-case' by depth and radius) centered on the vehicle descent axis. Realistic surface topologies including pre-existing craters or obstacles, like rocks, could be studied with a similar engineering model framework in the future. However, authors including Morris et al. (2015b) have found collisions between regolith particles within the plume flow to be a significant factor in promoting high-angle regolith transport. The JPL model framework does not account for such grain-grain collisions, the study of which at engineering scale would incur significant expenses in physics model development and computational time. Instead, particle initialization conditions were selected in order to replicate Apollo observations without directly representing their motivating physics – this approach could be improved in future work, and could be augmented by observations from additional landing vehicles.

Generally, particle impingement rates onto aft panels and active radiators were found to increase with decreasing altitude, with peak rates observed at 1.5 m. Generally, surfaces located 'lowest' on the descent element, i.e. closest to ground during landing, received most contamination – leveling mechanisms and other landing-site oriented surfaces were found to achieve relatively high impingement rates compared to aft panels and radiators during integrated landing sequences. Compared to flat planar landing sites at altitudes between 10 and 1.5 m, worst-case cratered and worst-case sloped surfaces at the closest-approach altitude were found to promote particle transport onto the descent element.

F. Induced Contamination Effects: Thermo-Optical Property Degradation

As discussed in Section III, lunar regolith and dust will meaningfully increase heat loads when deposited on typical thermal control surfaces by altering surface thermo-optical properties. The results from the characterization of lunar regolith and dust entrainment, transport and deposition onto Blue Moon descent element sensitive surfaces are inputs in a thermo-optical property degradation analysis. Computed particle surface concentrations are converted to *percent area coverage*, PAC, with the method of IEST-STD-1246E standard Annex B.[28] A rule-of-mixtures approach

is applied using the initial optical properties of the sensitive surface $\alpha_{initial}$ and optical properties of the transported contaminant α_{contam} in order to arrive at an estimated effective surface optical property α_{Eff}:

$$\alpha_{\text{Eff}} = [\alpha_{initial} * (1 - PAC)] + [\alpha_{contam} * PAC] \quad (1)$$

JPL has assembled analysis cases that correspond to regolith properties outlined in Section III. The values presented in Table 2 consider a generic range of particulate loadings, each with best- and worst-case regolith optical property assumptions, that together bound performance degradation of a radiator surface with properties defined by Blue Origin. Based on properties measured by Gaier et al. (2012), the best-case properties were defined as an absorptivity of 0.39 and an emissivity of 0.92; the worst-case as absorptivity of 0.75 and emissivity of 0.78. The analysis cases presented in Table 3 consider a generic range of particulate loadings and use regolith optical properties that correspond to the mean values for South Pole regolith (α=0.84, Ɛ=0.965). Mare region regolith cases were also assessed, but resulted in minor property differences when compared with corresponding South Pole cases.

In this example, we observe some property degradation differences between Tables 2 and 3 – i.e. between a model that applies regolith properties derived from a broad literature survey of collected regolith and simulant, or that instead applies properties derived instead from measurements of a specific lunar region. These differences increase with increasing PAC. Once a specific lunar landing region or site is selected for a mission, it may be beneficial to infuse whatever information is available about local regolith properties into such a model to reduce uncertainty.

Table 2. Example of thermo-optical property degradation calculations for radiator surfaces with partial coverage, surveying a range of regolith and simulant properties as applied in the Blue Moon model (2019–2020).

PAC	Best-case values			Worst-case values		
	Absorptivity	Emissivity	A / E	Absorptivity	Emissivity	A / E
1 %	0.192	0.861	*0.223*	0.196	0.859	*0.228*
3 %	0.196	0.862	*0.227*	0.207	0.858	*0.241*
5 %	0.2	0.863	*0.232*	0.218	0.856	*0.255*
15 %	0.22	0.869	*0.253*	0.274	0.848	*0.323*
30 %	0.25	0.878	*0.285*	0.358	0.836	*0.428*

Table 3. Example of thermo-optical property degradation calculations for radiator surfaces with partial coverage, using lunar South Polar regional properties from NASA SLS-SPEC-159 Revision I (Oct. 2021).[25]

PAC	Absorptivity	Emissivity	A / E
1 %	0.197	0.861	*0.228*
3 %	0.210	0.863	*0.243*
5 %	0.223	0.865	*0.257*
15 %	0.288	0.876	*0.328*
30 %	0.385	0.892	*0.432*

VI. Conclusion and Future Work

Plume-surface interactions and plume-induced contamination events pose inevitable threats to future landed lunar missions: mission objectives can be threatened during landing as the nominal operation of propulsion systems erodes regolith and transports and deposits material onto descent element and payload sensitive surfaces. Physics-based engineering models for plume effects during landings can provide valuable input to the design of landed vehicles and missions. JPL develops and applies such models to characterize plume-induced molecular and particulate deposition; hardware and instrument degradation due to, for instance, thermo-optical property changes; and landing site alteration. JPL analysis deliverables in support of Blue Moon included a description of the problem of lunar regolith erosion and particle transport in engine plumes during landing, including impingement and deposition onto descent element surfaces and optical effects of deposited lunar dust onto thermal control system radiators. This manuscript introduced an engineering model framework developed to characterize the plume-induced contamination effects of lunar landing

events and reviewed a reduced geometric model for the Blue Moon descent element; coupled CFD-DSMC models and flowfields for a Blue Moon dual-engine configuration at altitudes of 10, 5, 3, and 1.5 m; preliminary models for regolith erosion and particle mobilization, transport, and deposition; and a tool for use in the assessment of thermo-optical degradations of thermal control system radiators. Versions of this engineering model framework have already shown utility to other lunar landing programs. JPL has continued development of model capabilities for plume-surface interaction since the conclusion of Blue Moon analyses, and anticipates future work toward the adoption of two-way coupled schemes for gas dynamic solutions and granular solvers for modeling plume-induced erosive processes. The availability of additional data from terrestrial test programs and from future landed vehicles would be essential both to validate and to improve future engineering models for plume-surface interactions during lunar landings.

Acknowledgments

This work was performed at the Jet Propulsion Laboratory, California Institute of Technology, under a contract with the National Aeronautics and Space Administration. High Performance Computing (HPC) resources used in this investigation were provided by funding from the JPL Information and Technology Solutions Directorate. The authors would like to thank Rebekah L. Lam of JPL Chemical Propulsion for her contributions to preliminary versions of this work, and Drs. John R. Anderson and Gregory S. Shallcross of JPL Contamination Control Engineering for their helpful comments and ongoing development of certain models and techniques relevant to modeling lunar landings.

References

[1] Immer, C., Metzger, P., Hintze, P., Nick, A., Horan, R., "Apollo 12 Lunar Module exhaust plume impingement on Lunar Surveyor III," *Icarus,* Vol. 211, No. 2, 2011, pp. 1089-1102. https://doi.org/10.1016/j.icarus.2010.11.013

[2] Morris, A.B. "Simulation of Rocket Plume Impingement and Dust Dispersal on the Lunar Surface," Ph.D. Dissertation, Dept. of Aerospace Engineering and Engineering Mechanics, Univ. Texas at Austin, Austin, TX, 2012.

[3] Rahimi, A., Ejtehadi, O., Lee, K.H., Myong, R.S., "Near-field plume-surface interaction and regolith erosion and dispersal during the lunar landing," *Acta Astronautica*, Vol. 175, 2020, pp. 308-326. https://doi.org/10.1016/j.actaastro.2020.05.042

[4] Watkins, R., et al., "Understanding and Mitigating Plume Effects During Powered Descents on the Moon and Mars," 2021, *Planetary Science and Astrobiology Decadal Survey 2023-2032* Whitepaper #089. https://doi.org/10.48550/arXiv.2102.12312

[5] Morris, A.B., Goldstein, D.B., Varghese, P.L., Trafton, L.M. "Approach for Modeling Rocket Plume Impingement and Dust Dispersal on the Moon," *AIAA Journal of Spacecraft and Rockets,* Vol. 52, No. 2., 2015. https://doi.org/10.2514/1.A33058

[6] Lam, R.L., Maghsoudi, E., Hoey, W.A., "Numerical Study of Lander Engine Plume Impingement on the surface of Europa," *Proceedings of the 37th Joint Army Navy NASA Air Force (JANNAF) Exhaust Plume and Signatures Meeting*, JANNAF, Dayton, OH, 2019. https://doi.org/2014/46431

[7] Hoey, W.A., Lam, R.L., Wong, A.T., Soares, C.E., "Europa Lander Engine Plume Interactions with the Surface and Vehicle," *Proceedings of the IEEE Aerospace Conference*, IEEE, Big Sky, MT, 2020. https://doi.org/10.1109/AERO47225.2020.9172679

[8] Prem, P., Hurley, D.M., Goldstein, D.B., Varghese, P.L., "The Evolution of a Spacecraft-Generated Lunar Exosphere," *J. Geophysical Research: Planets*, 2020. https://doi.org/10.1029/2020je006464

[9] Zhang, H., et al., "The Investigation of Plume-Regolith Interaction and Dust Dispersal during Chang'E-5 Descent Stage," *Aerospace*, Vol. 9, No. 7., 2022. https://doi.org/10.3390/aerospace9070358

[10] Grabe, M., Soares, C.E., "Status and Future of Research on Plume Induced Contamination," *Proceedings of the 70th International Astronautical Congress*, IAF, Washington, D.C., 2019.

[11] Gaier, J.R., "The Effects of Lunar Dust on EVA Systems During the Apollo Missions," NASA TM-2005-2013610/REV1, Cleveland, OH, Apr. 2007.

[12] *Analysis of Surveyor 3 Material and Photographs Returned by Apollo 12*, NASA SP-284, Washington, D.C., Jan. 1972.

[13] Bird, G.A., *Molecular Gas Dynamics and the Direct Simulation of Gas Flows*, Oxford Univ. Press, New York, NY, 1994.

[14] LeBeau, G.J., "A Parallel Implementation of the Direct Simulation Monte Carlo Method," *Computer Methods in Applied Mechanics and Engineering*, Vol. 174, Nos. 3-4, 1999, pp. 319-337. https://doi.org/10.1016/S0045-7825(98)00302-8

[15] Lumpkin, F.E., Marichalar, J.J., Stewart, B.D., "High-Fidelity Simulations of Plume Impingement to the International Space Station," *Proceedings of the 33rd Joint Army Navy NASA Air Force (JANNAF) Exhaust Plume and Signatures Meeting*, JANNAF, Monterey, CA, 2012.

[16] Mehta, M., Sengupta, A., Renno, N.O., Van Norman, J.W., Huseman, P.G., Gulick, D.S., Pokora, M., "Thruster Plume Surface Interactions: Applications for Spacecraft Landings on Planetary Bodies," *AIAA Journal*, Vol. 51, No. 12, 2013, pp. 2800-2818. https://doi.org/10.2514/1.J052408

[17] Roberts, L., "The Action of a Hypersonic Jet on a Dust Layer," *31st Annual Meeting of the Institute of Aerospace Sciences*, IAS, Paper 63-50, New York, NY, Jan. 1963.

[18] Metzger, P.T., et al., "Scaling of Erosion Rate in Subsonic Jet Experiments and Apollo Lunar Module Landings," *12th Biennial International Conference on Engineering, Construction, and Operations in Challenging Environments, Earth and Space 2010,* American Society of Civil Engineers, Honolulu, HI, Mar. 2010. https://doi.org/10.1061/41096(366)21

[19] Metzger, P.T., Lane, J.E., Immer, C.D., "Modification of Roberts' Theory for Rocket Exhaust Plumes Eroding Lunar Soil," *11th ASCE Aerospace Division International Conference, Earth and Space 2008,* American Society of Civil Engineers, Long Beach, CA, Mar. 2008. https://doi.org/10.48550/arxiv.2104.05198

[20] Brieda, L., "Numerical Model for Molecular and Particulate Contamination Transport," *Journal of Spacecraft and Rockets*, Vol. 56, No. 2, 2018. https://doi.org/10.2514/1.A34158

[21] Anderson, J.R., Hoey, W.A., Alred, J.M., Soares, C.E., Brieda, L., "Space Launch Vehicle Transient Particle Redistribution Modeling and Implications for Optically Sensitive Payloads," *Systems Contamination: Prediction, Control and Performance*, SPIE, vol. 11489, Aug. 2020. https://doi.org/10.1117/12.2567765

[22] Heiken, G.H., Vaniman, D.T., French, B.M., *Lunar Sourcebook, A User's Guide to the Moon*, Cambridge Univ. Press, 1991.

[23] Colwell, J.E., Batiste, S., Horanyi, M., Robertson, S., Sture, S., "Lunar Surface: Dust Dynamics and Regolith Mechanics," *Reviews of Geophysics*, Vol. 45, No. 2, 2007. https://doi.org/10.1029/2005RG000184

[24] Gaier, J.R., Ellis, S., Hanks, N., "Thermal Optical Properties of Lunar Dust Simulants," *Journal of Thermophysics and Heat Transfer*, Vol. 26, No. 4, 2012. https://doi.org/10.2514/1.T3838

[25] *SLS-SPEC-159, Cross-Program Design Specification for Natural Environments (DSNE)*, Rev. I, NASA, Oct. 2021.

[26] Morris, A.B., Goldstein, D.B., Varghese, P.L., Trafton, L.M. "Lunar Dust Transport Resulting from Single- and Four-Engine Plume Impingement," *AIAA Journal*, Vol. 54, No. 4, 2015. https://doi.org/10.2514/1.J054532

[27] Hoey, W.A., Trafton, L.M., Ackley, P.C., Goldstein, D.B., Varghese, P.L., "Variations in the Canopy Shock Structures of Massive Extraterrestrial Plumes: Parametric DSMC Simulation of 2007 Tvashtar Observations," *Icarus*, Vol. 363, No. 114431, 2021. https://doi.org/10.1016/j.icarus.2021.114431

[28] *Product Cleanliness Levels – Applications, Requirements, and Determination*, Insitute of Environmental Sciences and Technology, IEST-STD-CC1246E, Feb. 2013.